



1 West Antarctic Ice Retreat Temporarily Halted with Transient 2 Rheology in Future Climate Projections

3 Allie N. Coonin¹, B Parazin², Harriet C.P. Lau¹, Natalya Gomez²

4 ¹Department of Earth, Environmental, and Planetary Sciences, Brown University, 167 Thayer St., Providence, RI
5 02912, USA

6 ²Department of Earth and Planetary Sciences, McGill University, 3450 University St., Montreal Quebec, Canada H3A
7 0E8

8
9 *Correspondence to:* Allie N. Coonin (allie_coonin@brown.edu)

10 **Abstract.** Projections of sea-level change and Antarctic Ice Sheet (AIS) stability under
11 anthropogenic climate change hinge upon accurately describing physical feedbacks that link ice
12 dynamics (marine and terrestrial) with the gravitational, rotational and deformational response of
13 the solid Earth to ice and ocean loading changes. In turn, the rate of AIS melting can lower the
14 rate of global mean temperature rise, by promoting sea ice growth and amplifying Earth's
15 albedo. The marine West Antarctic Ice Sheet (WAIS) is vulnerable to runaway grounding line
16 retreat. However, the rapid viscoelastic rebound of the bedrock in response to ice retreat has been
17 shown to stabilize its grounding line, aided by the low-viscosity mantle beneath the WAIS. Such
18 bedrock deformation is typically modelled with idealized Maxwell viscoelasticity, despite that
19 rock deformation experiments show that additional “transient” creep mechanisms occur over
20 societally relevant (~decadal-centennial) timescales that are missing from the Maxwell model.
21 Here, we simulate future AIS evolution, coupled with self-consistent solid Earth deformation and
22 sea level change, for various emissions scenarios (RCP 2.6, 4.5, 8.5), incorporating transient
23 deformation. This more complete treatment of solid Earth deformation delays grounding line
24 retreat as compared to Maxwell projections, with differences of tens of kilometres persisting for
25 decades at Pine Island and Thwaites Glaciers. Though transient deformation slows glacier
26 retreat, it is unable to prevent the bulk of ice loss and sea-level rise on longer, centennial
27 timescales. Even still, deviations in AIS meltwater flux with transient deformation could affect
28 the pace of global temperature rise in climate model predictions.

29
30
31 **Short Summary.** Sea level change and ice sheet stability depend on how Earth's bedrock warps
32 as ice melts. Rock experiments show that traditional models for bedrock deformation leave out
33 important processes relevant for modern ice loss. We simulate the coevolution of the Antarctic
34 ice sheet and global sea level under various climate change scenarios. When more realistic
35 bedrock behavior is considered, Antarctic ice retreat is delayed. Ultimately, this has implications
36 for the rate of global temperature rise.

37



38 Main Text

39 1. Introduction

40 Predictions of ice sheet and sea-level change in response to various trajectories of atmospheric
41 carbon emissions have demonstrated the potential for dramatic ice retreat in West Antarctica
42 (Deconto & Pollard, 2016; Deconto et al., 2021; Kopp et al., 2017). This vulnerability to extreme
43 ice loss is largely because the bedrock underneath the marine-based West Antarctic Ice Sheet
44 (WAIS) deepens from the margins toward the ice sheet interior, which predisposes the WAIS to
45 runaway retreat via the Marine Ice Sheet Instability (Schoof, 2007; Thomas, 1979; Weertman,
46 1974). The flux through the grounding line, the location at which the ice sheet begins to float
47 because it is too thin to displace the entire weight of the water column, has strong sensitivity to
48 the thickness of ice at the grounding line (with outflow proportional to ice thickness to the power
49 ~ 5 , Schoof, 2007.) Therefore, on such retrograde bed slopes, even a small perturbation can
50 trigger unstable collapse as the grounding line retreats to a location with deeper bedrock and
51 greater ice thickness. This greater grounding line ice thickness heightens ice loss through the
52 grounding line, promoting continued retreat until the bed begins to slope up or the grounding line
53 becomes pinned on a sill. Grounding line migration is further complicated by time-evolving and
54 highly spatially variable basal conditions due to processes like subglacial water flow and the
55 formation of subglacial landforms, allowing for other possible modes such as irregular
56 oscillations between advance and retreat (Sergienko & Wingham, 2024).

57 By nature of this dependence on bedrock topography and slope, marine ice sheet retreat is
58 a critical avenue for dynamical feedback between ice sheet evolution and solid Earth
59 deformation and sea level (e.g., Gomez et al., 2010). The redistribution of ice and ocean over
60 Earth's surface in response to an evolving climate will induce gravitational, rotational, and
61 deformational effects on the solid Earth, collectively termed Glacial Isostatic Adjustment (GIA),
62 which modify the timing and pattern of sea level and bedrock elevation change (Mitrovica et al.,
63 2001). Through the Marine Ice Sheet Instability mechanism discussed above, when sea level
64 rises at a marine grounding line (e.g. from far-field ice loss), this will accelerate ice loss across
65 the grounding line and promote grounding line retreat. On the other hand, local ice loss drives
66 local sea level fall due to solid Earth uplift and gravitational drawdown of the sea surface, which
67 slows ice loss and stabilizes the grounding line (Barletta et al., 2018; Gomez et al., 2015; Larour
68 et al., 2019). Changes in bedrock elevation from GIA can also impact ice sheet mass balance
69 through modulation of ice surface temperature, with the potential to reduce surface melting
70 and/or increase the amount of precipitation that falls as snow, aiding in mass accumulation (Zeit
71 et al., 2022). Studies investigating such feedbacks between solid Earth deformation, sea level,
72 and ice sheet evolution have suggested that the coupling acts to reduce changes in ice volume
73 over timescales of full glacial cycles (Abe-Ouchi et al., 2013; Gomez et al., 2013; Han et al.,
74 2021).

75 The calculation of gravitationally self-consistent sea-level change due to the
76 redistribution of ice and ocean mass at Earth's surface and consequently, its potential to
77 influence ice sheet evolution, is contingent on the deformational response of the solid Earth.
78 Typically, GIA models assume an idealized linear viscoelastic Maxwell rheology, which
79 deforms by an instantaneous and fully recoverable elastic response and a delayed, irrecoverable
80 viscous response, characterized by the mantle's elastic modulus and viscosity. The viscous
81 response of a mantle with higher viscosity will be delayed longer. For such deformation, the



82 characteristic timescale of viscoelastic deformation is known as the so-called Maxwell time, τ_M
83 (defined simply by the ratio between a material's viscosity to its elastic modulus). Intuitively,
84 any surface loading changes will induce viscoelastic deformation over timescales $\approx \tau_M$. For
85 rapid changes where loading timescales are $\ll \tau_M$, elastic deformation dominates and oftentimes
86 deformation is modelled with an entirely elastic mantle. For ice mass changes associated with
87 modern climate change, this is often the case since τ_M for the bulk mantle ranges between
88 approximately 500 to 10,000 years (K. Hansen et al., 2021; Spada et al., 2012; Whitehouse et al.,
89 2012). In contrast, the full viscoelastic response is modelled in the case of GIA over ice age
90 cycles (with timescales of 1000s to 10,000s of years). In locations like West Antarctica,
91 however, the underlying mantle is characterized by relatively low mantle viscosity with $\tau_M \approx 10$
92 to 100 years (Barletta et al., 2018; Lloyd et al., 2020; Lucas et al., 2024), and such an assumption
93 of mantle elasticity cannot be made. And thus, even for some modern cases, the viscoelastic
94 deformation must be accounted for. To account for both Maxwell viscoelasticity and the large
95 geographical variations in mantle viscosity, recent studies developed coupled models of future
96 Antarctic ice sheet and sea level evolution that incorporate lateral variations in Earth's viscosity
97 structure (Gomez et al., 2024; van Calcar et al., 2025). While they assume Maxwell viscoelastic
98 Earth rheology, Gomez et al. (2024) demonstrated that the consideration of 3D Earth structure
99 could reduce the Antarctic global mean sea level (GMSL) contribution by 2500 relative to that
100 predicted with radially symmetric Earth structure by up to 40%.

101 In this paper, we argue that even Maxwell viscoelasticity is insufficient to characterize
102 solid Earth deformation, especially on modern (decadal to centennial) timescales. Evidence for
103 this largely stems from the rock physics community, where experiments confirm that non-elastic
104 deformation mechanisms are activated even across these timescales (decadal to centennial) and
105 beyond (e.g., Faul & Jackson, 2011; Gribb & Cooper, 1998; McCarthy et al., 2011; Yamauchi &
106 Takei, 2016). The associated strains of such models are non-instantaneous, but recoverable, and
107 we will collectively term such models as transient models (Havlin et al., 2021; Lau et al., 2021).
108 Indeed, by incorporating a variety of transient models, a growing body of literature has
109 demonstrated the importance of moving away from Maxwell viscoelasticity on decadal-
110 centennial ice mass changes in several contexts (e.g. Adhikari et al., 2021; Coonin et al., 2025,
111 Ivins et al., 2023; Lau, 2024).

112 The elastic, transient viscous, and Maxwell steady state components of strain add
113 together to describe the total deformation response. Hence, if the Earth is more compliant over
114 shorter timescales, regardless of the assumed viscosity structure of the mantle, the magnitude and
115 timing the solid Earth response to ice and ocean load changes and consequently, sea level and
116 topography will differ by as much as meters (Coonin et al., 2025; Lau, 2023). In particular,
117 decadal to centennial timescales of modern ice loss and potentially even more rapid projections
118 of ice loss into the future will activate these transient deformation mechanisms. However, the
119 effect of transient viscous deformation in coupled simulations of future Antarctic ice evolution
120 has yet to be investigated.

121 Inspired by the coupled ice sheet and sea-level dynamics study of Gomez et al. (2024)
122 discussed above, which incorporated Maxwell viscoelastic deformation, here we modify their
123 approach by considering transient viscoelastic deformation. While Gomez et al. (2024) showed
124 that laterally varying properties clearly play an important role in coupled global sea level-
125 Antarctic ice sheet evolution, such models with 3D earth structure require significantly greater
126 computational power and we do not take this route, instead opting for 1D (i.e., depth dependent
127 only) mantle viscoelastic structure. Not only is this computationally more feasible, but it also



128 allows us to isolate the effect that transient deformation alone has in modulating the solid Earth's
129 response to modern timescales of ice loss. In this study, we explore the consequences of
130 incorporating more realistic solid Earth rheology, namely transient rheology, in coupled ice
131 sheet-sea level dynamics. We examine the effect of transient solid Earth rheology on the
132 evolution of the Antarctic ice sheet for various emissions scenarios (RCPs 2.6, 4.5, and 8.5;
133 IPCC, 2014), namely because we expect that transient deformation will be more sensitive to the
134 rates of ice volume changes than a typical Maxwell model over the relevant timescales (decades
135 to centuries).
136

137 2. Methods

138 2.1 Coupled ice sheet-sea level modelling

139 We run forward simulations of Antarctic Ice Sheet evolution using the PSU 3D ice sheet shelf
140 model (Pollard & Deconto, 2012; Pollard et al., 2015) coupled with solving the 1D
141 gravitationally self-consistent sea-level equation, accounting for gravitational, deformational and
142 rotational effects from glacial isostatic adjustment using the algorithm outlined in Kendall et al.
143 (2005). Within this algorithm, the calculation of deformation routinely adopts Maxwell
144 viscoelastic Earth rheology (Gomez et al., 2015; Han et al., 2022; Pollard et al., 2017), but has
145 more recently been adapted to consider the effects of transient viscoelastic solid Earth rheology
146 (Lau, 2024). To the authors' best knowledge, transient rheology has only been considered in
147 coupled ice sheet-sea level modelling once before and only very recently, where Caron et al.
148 (2025) modify the coupled Ice Sheet-Sea-Level System Model (ISSM) to incorporate the
149 Extended Burgers viscoelastic model (Faul & Jackson, 2015) for solid Earth deformation. Here,
150 we take this further and consider a realistic climate scenario which we describe below.

151 Required inputs for the ice sheet model are the bedrock topography, basal sliding
152 coefficients, geothermal heat flux, sea-level, and – as just mentioned – air temperature and
153 precipitation outputs from a climate model of the RCP climate projections (IPCC, 2014) as in
154 Gomez et al. (2024) and Deconto et al. (2021). Required inputs for the sea level model include
155 the initial bedrock topography, a prescribed loading history, and the Love numbers
156 corresponding to the chosen radially varying viscoelastic Earth model (see Fig. S2; Kendall et
157 al., 2005). Love number theory is a Green function approach to determining the viscoelastic
158 deformation of the solid Earth and the Earth's gravity field, given a surface load history. The ice
159 sheet and sea-level models communicate via offline coupling with a timestep of 10 years. That
160 is, under the prescribed climate forcing, the ice sheet model runs with the specified internal time-
161 stepping (here set to ~18 days as in DeConto et al., 2021; Fig. S4) until the coupling time is
162 reached. At this point, the associated ice volume changes are then fed into the sea-level model to
163 calculate changes in sea-level and bedrock topography. These fields are sent back to the ice
164 model, thereby impacting ongoing ice sheet evolution. The coupling time step of 10 years was
165 chosen to balance resolution with computation time, since sensitivity tests for the coupling time
166 step showed minimal differences for the choice of 25-, 10-, or 2-year coupling time steps (see
167 Fig. S3). Forward calculations of global sea-level change are performed to spherical harmonic
168 degree 512 (~80 km resolution), and a spatial resolution of 10 km is used within the ice sheet
169 model. Unfortunately, finer spatial resolutions are computationally infeasible for continental-
170 scale calculations (Gomez et al., 2024). To isolate the effects of the choice of solid Earth
171 rheology on Antarctic Ice Sheet evolution, we hold ice volume and extent constant over the



172 remainder of the globe, hence any changes in GMSL are the result of Antarctic Ice Sheet
173 changes only.

174 **2.2 Ice sheet dynamics**

175 The dynamic ice component is a hybrid ice sheet-shelf model employing the shallow ice
176 and shallow shelf approximations for ice flow (which account for vertical shearing and
177 longitudinal stretching respectively), ensuring computational feasibility for continental-scale
178 simulations (Pollard & DeConto, 2012). A modified version of the Schoof (2007)
179 parametrization for ice flux through the grounding line is adopted, allowing for evolving
180 grounding line position according to the Marine Ice Sheet Instability (MISI) and self-consistency
181 with the basal shear stress condition at the grounding line (Pollard & DeConto, 2012; Schoof,
182 2007). Surface mass balance is calculated by a positive-degree day scheme using RCP
183 temperature and precipitation forcings. Sub-ice oceanic melting and calving at ice shelf edges are
184 additional considerations in the ice sheet mass balance. Calving, though still poorly understood,
185 is an important consideration for tidewater glaciers and ice shelves because floating ice can
186 stabilize grounded ice upstream by means of buttressing at the grounding line (Gudmundsson,
187 2013; Sergienko, 2025). We consider two endmembers to describe ice loss through calving – a
188 parametrization based on the large-scale stress field of the ice sheet where calving is related to
189 the thickness of the ice shelf and is proportional to the positive divergence of floating ice
190 velocity for thicker ice shelves (Nick et al., 2010) and the highly debated Marine Ice Cliff
191 Instability (MICI), which is a physical treatment to account for hydrofracturing due to surface
192 melt and failure of vertical cliff faces (Bassis et al., 2021; Golledge & Lowry, 2021; Pollard et
193 al., 2015). The main results presented in this paper reflect the former, though we explore a
194 possible scenario of accelerated retreat due to the MICI (see Section 4.2).

195 **2.3 Solid Earth Structure and Rheology**

196 While we focus on West Antarctica in the Main Text, we consider two distinct 1D Earth models
197 to represent the geological dichotomy of the Antarctic continent, where East Antarctica is
198 characterized by cold cratonic structure and West Antarctica is characterized by thin lithosphere
199 underlain by relatively warm mantle. For both models, however, we assume the elastic and
200 density properties based on the Preliminary Reference Earth Model (Dziewonski & Anderson,
201 1981). The elastic properties of the mantle are much less sensitive to temperature differences
202 than the viscous properties, where the steady state, or Maxwell, viscosities differ by orders of
203 magnitude. In accordance with East Antarctic structure, we assume a steady state viscosity
204 profile (hereafter referred to as η_H , as in higher steady state viscosity model), which is comprised
205 of a 96 km-thick lithosphere, an upper mantle viscosity of $10^{20} \text{ Pa} \cdot \text{s}$, and a lower mantle
206 viscosity of $5 \times 10^{21} \text{ Pa} \cdot \text{s}$ ($> 670 \text{ km}$ depth). To reflect West Antarctic mantle structure, we
207 assume a reduced steady state viscosity model (hereafter referred to as η_L) with a 50 km-thick
208 lithosphere overlying a zone with reduced viscosity down to 400 km depth with a viscosity of
209 $10^{19} \text{ Pa} \cdot \text{s}$, a viscosity of $2 \times 10^{20} \text{ Pa} \cdot \text{s}$ for the remainder of the upper mantle, and a lower mantle
210 viscosity ($> 670 \text{ km}$ depth) of $3 \times 10^{21} \text{ Pa} \cdot \text{s}$. To be clear, in order to model the entire continent
211 self-consistently in a way that captures the East-West dichotomy, we would require a 3D model
212 of GIA (as in Gomez et al., 2024). As mentioned, this is computationally expensive and we
213 emphasize that our approach (i.e., to run full simulations with two distinct 1D Earth models) is a



214 reasonable approximation to model each side of the continent, since our focus, as we shall see,
215 will be on deformation in the direct vicinity of each region.

216 With these mantle properties, we calculate the viscoelastic Love numbers using the
217 methodology outlined in Lau (2024). We do this for both a Maxwell viscoelastic rheology –
218 which we will treat as our reference calculation – and for a transient viscoelastic rheology,
219 adopting the empirical law of Yamauchi and Takei (2016) for both 1D Earth models. The
220 Yamauchi and Takei (2016) transient rheology model accounts for the observed weakening
221 across timescales spanning the elastic to steady state and can conveniently be scaled to a
222 particular reference Maxwell model (see SM-1 for more details on these models). We compare
223 the coupled ice sheet-sea level modelling results for simulations with the same steady state Earth
224 structure but with Maxwell versus transient viscoelastic solid Earth rheology to assess the impact
225 of including transient viscoelastic deformation on sea level and ice sheet evolution for the
226 prescribed climate forcing between 1950 to 2500 (RCP 2.5, RCP 4.5, RCP 8.5; IPCC, 2014). An
227 Earth with transient solid Earth rheology will be more sensitive to the pace of ice melting over
228 timescales smaller than typical Maxwell relaxation times, so, given that our planet’s actual
229 trajectory of radiative forcing is unknown, we explore multiple climate change scenarios and also
230 modify the rate of ice loss in each climate scenario further by invoking the rapid ice loss via
231 MICI.

232 **2.4 Calculating Antarctic Global Mean Sea Level Contribution**

233 Mass balance can be used to estimate the GMSL contribution associated with the simulated co-
234 evolution of ice sheet and sea-level change. In consideration of the effects of transient Earth
235 deformation on predictions of the Antarctic contribution to GMSL, we neglect steric changes and
236 adopt the modified volume above floatation (VAF) method described in Equation (1) of Gomez
237 et al. (2024), which is applicable for cases where there are minimal changes in ice sheets and/or
238 shorelines outside of Antarctica. This formulation accounts for water expulsion from regions of
239 Antarctica below sea level to the remainder of the ocean. While globally, the ice mass lost will
240 be equal to the mass gained by the ocean, in this paper we consider the Antarctic GMSL
241 contribution to be the global average sea level rise in the rest of the world due to Antarctic ice
242 loss and the gravitational, rotational, and deformational feedbacks from GIA. We present the
243 deviations in GMSL predictions, uplift, ice volume, and marine grounding line dynamics in West
244 Antarctica due to the inclusion of transient Earth deformation in the following section.

245 **3. Results**

246 Figure 1 shows the initial ice configuration for all simulations (1950 CE; Fig. 1a) and the change
247 in ice thickness between 1950 and 2500 CE across West Antarctica the η_L steady state viscosity
248 with Maxwell solid Earth rheology, our reference case (Fig. 1b.i RCP 2.6; Fig. 1b.ii RCP 4.5;
249 Fig. 1b.iii RCP 8.5). We note that in all map figures, the unshaded region is that in which the
250 background viscoelastic structure is appropriate (e.g., for an unshaded Western Antarctic region,
251 the simulation adopted the η_L steady state profile). Projected ice loss under RCP 8.5 in West
252 Antarctica is drastic, with ice thickness losses as large as 2 km and near-complete collapse of the
253 Filchner-Ronne and Ross ice shelves (grey fill in Fig. 1a to reduced extent in Fig 1b.iii). While
254 floating ice does not impact GMSL, loss of ice shelves can reduce buttressing of upstream
255 grounded ice, leading to reductions in grounded ice volume and consequently, GMSL rise. In
256 addition to loss of floating ice, grounded ice margins of the WAIS undergo notable retreat (Fig.



257 1b; compare grey contour of initial grounded ice margins and solid black contour outlining final
258 grounded ice margins in the Maxwell model). Grounded ice loss is particularly severe in the
259 Amundsen Sea Embayment (ASE), which encompasses the swiftly deglaciating Pine Island
260 (transect A-A'; Fig. 1a) and Thwaites Glacier (transect B-B'; Fig. 1a). The near-complete
261 collapse of the ASE in RCP 8.5 disconnects the grounded ice of the Antarctic Peninsula from the
262 remainder of the continent. The starting point of the glacier transects (circle markers A, B) are
263 located along the initial grounded ice margins. Small yellow areas along the Maxwell model in
264 the ASE region indicate places where the final grounded ice margins in the transient model
265 extend further outward than those within the Maxwell model. There is noticeably less grounding
266 line retreat in the ASE under the more moderate emissions scenarios, RCPs 2.6 and 4.5,
267 however, if the parametrization of MICI is applied within the coupled model, the ice loss
268 exceeds that of RCP 8.5 without MICI for both RCP 2.6 and 4.5, resulting in near-total collapse
269 of the ASE and the interior of the WAIS (see SM-6).

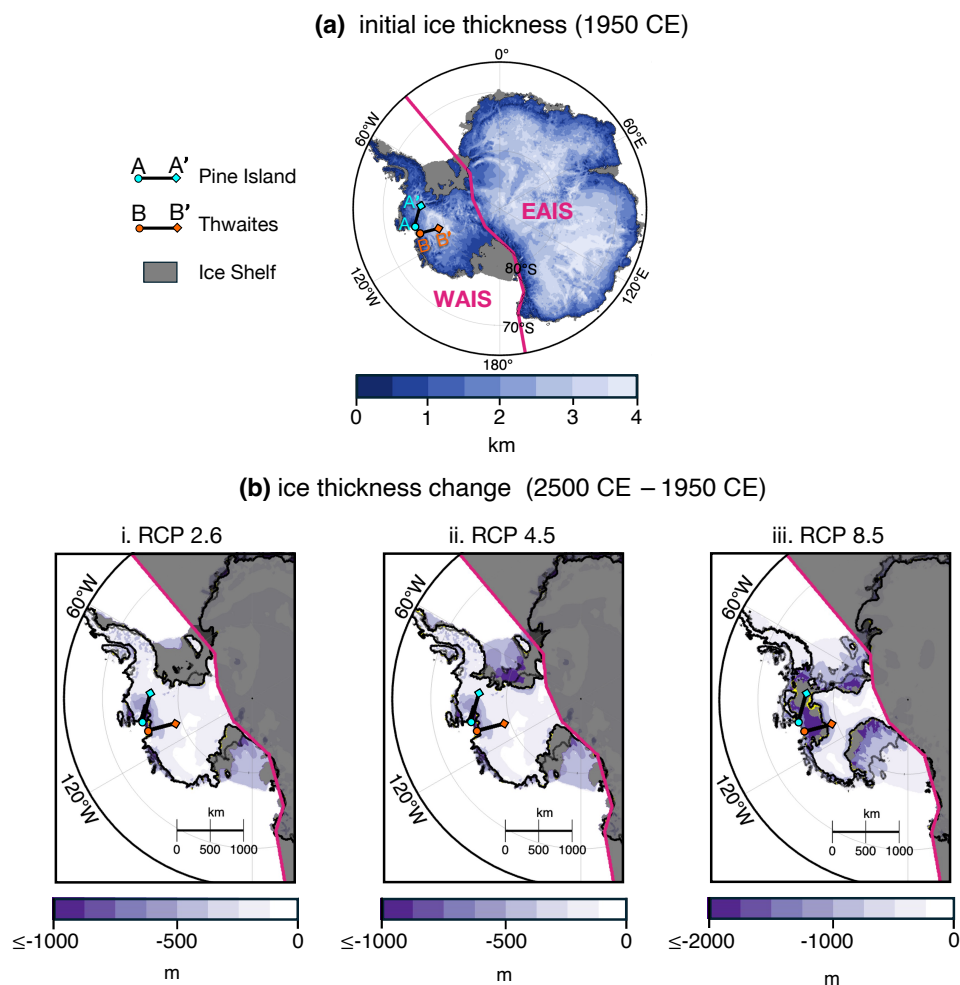


Figure 1. Maxwell Model Ice Thickness Change: (a) initial ice sheet configuration and ice shelf extent at 1950 CE. (b) total change in ice thickness from 1950 CE to 2500 CE in West Antarctica with the η_L Maxwell Earth model for RCP 2.6 (b.i), RCP 4.5 (b.ii), and RCP 8.5 (b.iii). Solid contours outline initial (dark grey) and final (black) grounded ice extent in the Maxwell model. The final grounded ice extent in the transient model is contoured in yellow, indicating areas of additional grounded ice extent in the transient model, compared to the Maxwell model (b.iii). Pink line indicates division between East Antarctica and West Antarctica used in this study. Transsects A-A' (cyan markers) and B-B' (orange markers) cut through Pine Island and Thwaites glaciers, respectively. Solid grey fill in (b) indicates final ice shelf extent.

270 Once more, the Maxwell model results presented in Fig. 1 serve as a reference for solid
 271 Earth–ice sheet feedbacks without accounting for transient Earth deformation. We compare the
 272 effect of including transient Earth deformation on bedrock elevation and ice thickness relative to
 273 the reference Maxwell model at 2500 CE in Fig. 2. Regardless of the choice of solid Earth
 274 rheology, the largescale patterns of solid Earth deformation consist of uplift across West



275 Antarctica and subtle subsidence with pockets of uplift around marine outlet glaciers in East
 276 Antarctica. However, the magnitudes of vertical displacement are greater in the transient models
 277 for nearly the entirety of the continent, compared to that of the Maxwell model. Under RCP 8.5,
 278 the ASE is uplifted by an additional ~25 m when accounting for transient Earth deformation (~10
 279 m for RCPs 4.5 and 2.6; Fig. 2c,e).
 280

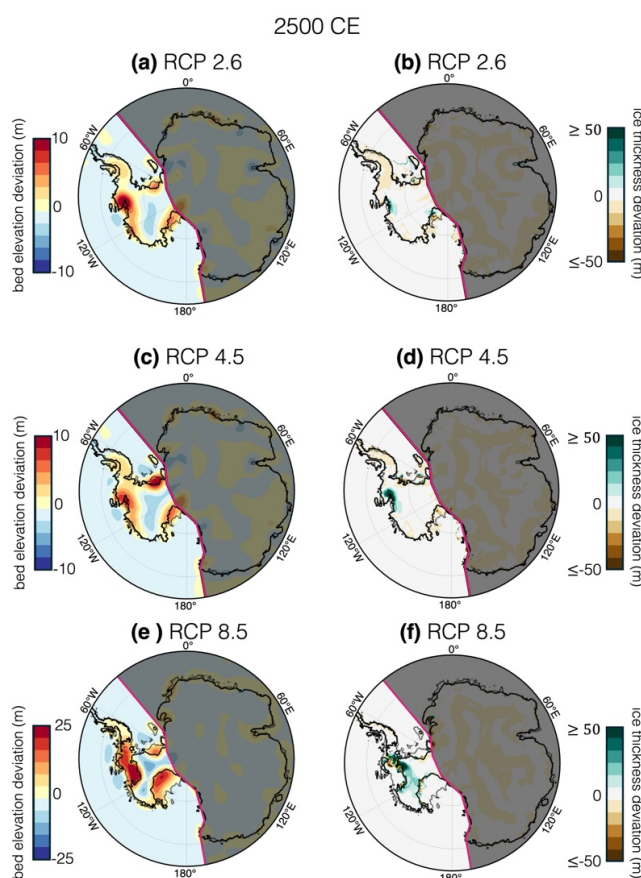


Figure 2. Bedrock and Ice Thickness Deviation (Transient minus Maxwell) (a),(c),(e) Difference between bedrock elevation of transient and Maxwell Earth rheology simulations at 2500 CE in West Antarctica for (a) RCP 2.6 and (c) RCP 4.5, and (e) RCP 8.5 respectively. (b),(d),(f) Difference between final ice thickness of transient and Maxwell Earth rheology simulations at 2500 CE in West Antarctica for (b) RCP 2.6 and (d) RCP 4.5, and (f) RCP 8.5 respectively.

281 3.1 Slowdown of grounding line retreat

282 Fig. 3 compares the relative pace of grounding line retreat in Maxwell versus transient models
 283 under RCP 8.5 (IPCC, 2014) at Pine Island (vertical lines, Fig. 3a,c) and Thwaites Glaciers (Fig.



284 3b,d). Along both glacier transects, the transient and Maxwell models are similar until around
 285 2300 CE, after which, there is observable deviation in the relative pace of grounding line retreat.
 286 Though, regardless of the rheology, the grounding line tends to become pinned along bumps in
 287 the bedrock or locations where the slope changes from retrograde to prograde, grounding line
 288 retreat at both glaciers in the transient model is delayed by decades or more relative to the
 289 Maxwell model. For every time slice in Fig. 3, the grounding line in the Maxwell model has
 290 retreated further upstream than in the transient model, with deviations in grounding line position
 291 greater than 30 km (RCP 8.5).
 292

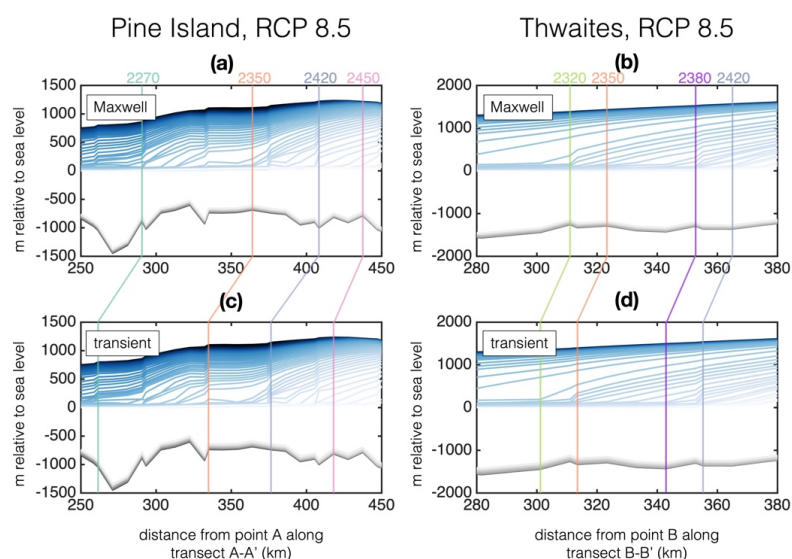


Figure 3. RCP 8.5 Grounding Line Retreat at Pine Island and Thwaites Glacier (a),(c) Evolution of bedrock surface (dark grey to light grey) and ice sheet surface (dark blue to light blue) elevation across Pine Island Glacier (Transect A-A', Figure 1a) considering Maxwell (a) vs. transient (c) viscoelastic solid Earth deformation. (b),(d) As in (a) and (c) but for Thwaites Glacier (Transect B-B', Fig. 1a). Connecting lines plotted in distinct colours indicate grounding line position at the indicated times within the simulation. At each illustrated time slice in the figure, the transient Earth simulation has undergone less retreat than the reference simulation considering only Maxwell viscoelastic deformation. All results shown adopt η_L steady state profile.

293 Fig. 4 demonstrates a similar progression at Pine Island glacier for RCPs 2.6 and 4.5,
 294 with more grounding line retreat at a given time within the Maxwell simulation than the transient
 295 simulation. In fact, the total distance of grounding line retreat by the year 2500 along the Pine
 296 Island glacier transect in the transient model is less than that of the Maxwell model (by ~10 km
 297 and 20 km for RCPs 2.6 and 4.5, respectively). In the last ~150 years of the coupled ice sheet-sea
 298 level evolution, grounding line retreat is significantly delayed in the transient model compared to
 299 the Maxwell model at Pine Island Glacier in all RCPs (Supplementary Movies 2-4). The same is
 300 true at Thwaites Glacier in RCP 8.5, though in the more moderate emissions scenarios there is
 301 little to no deviation in Thwaites Glacier grounding line retreat with transient rheology
 302 (Supplementary Movie 1). We emphasize that the marine outlet glaciers of the WAIS are broad
 303 spatial features, and we only show the grounding line migration through time along the transects



304 described in Fig. 1 in the cross-sections (Figs 3 and 4). The deviations in the spatial pattern of
 305 retreat of marine outlet glaciers are more complex, as illustrated by the areas where the grounded
 306 ice margins vary between the transient and Maxwell models off-transect in Figs 1 and 2 (yellow
 307 fill).
 308

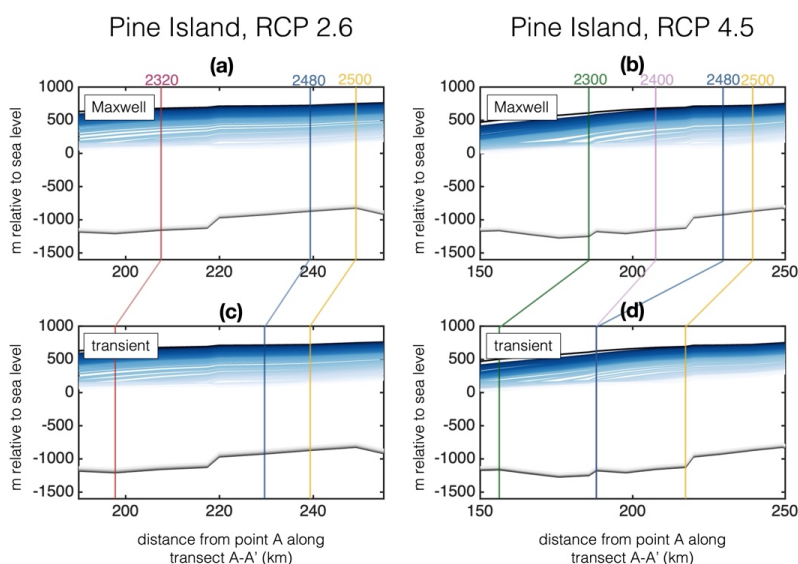


Figure 4. Grounding Line Retreat at Pine Island Glacier in RCP 2.6 and RCP 4.5 (a),(c) Evolution of bedrock surface (dark grey to light grey) and ice sheet surface (dark blue to light blue) elevation across Pine Island Glacier (Transect A-A', Fig. 1a) under RCP 2.6 considering Maxwell (a) vs. transient (c) viscoelastic solid Earth deformation. (b),(d) As in (a) and (c) but for RCP 4.5 climate forcing. At each time slice for either glacier transect, the transient Earth simulation has undergone less retreat than the reference Maxwell Earth rheology simulation. All results shown adopt the low steady state viscosity profile, to mirror West Antarctic Earth structure.



309 Moving to a continent-scale view of the predicted deformation and sea-level change, Fig.
 310 5 displays maps of the absolute value of bedrock uplift rate in the Maxwell model (left panels)
 311 and the deviation in uplift rate between the transient and Maxwell models (right panels) in West
 312 Antarctica at 2300 CE (here, uplift rate is defined as the radial displacement of the solid Earth
 313 surface over a change in time step.)
 314

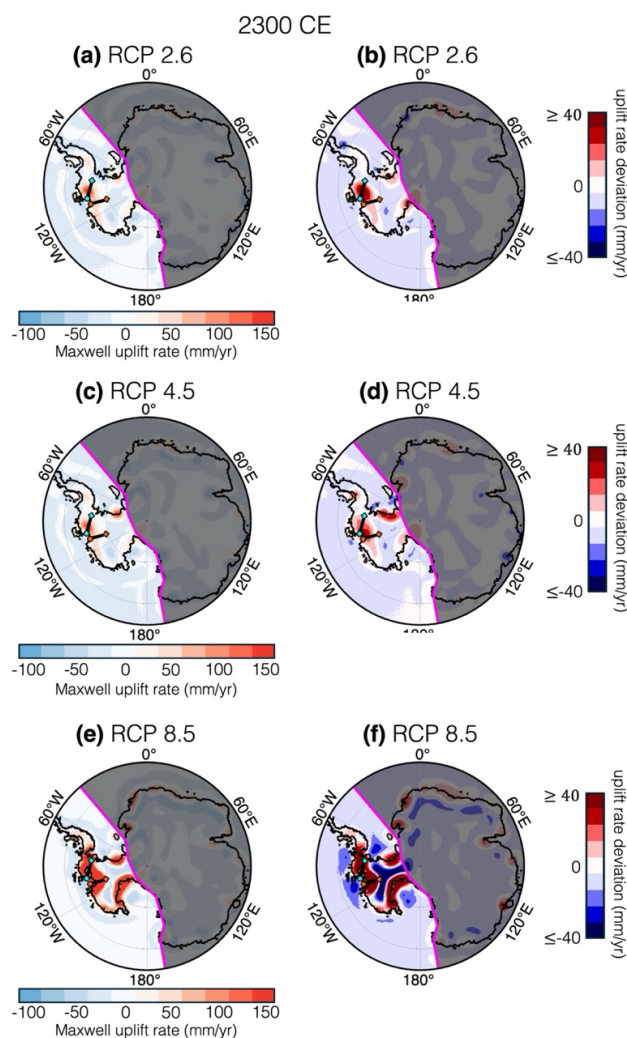


Figure 5. Vertical Bedrock Displacement Rate Deviation (Transient–Maxwell) (a),(c),(e) Uplift rate in mm/yr in the reference Maxwell simulation with low steady state viscosity profile for RCP 2.6, 4.5, and 8.5, respectively. (b),(d),(f) Difference in uplift rate (transient minus Maxwell) with the low steady state viscosity profile for RCP 2.6, 4.5, and 8.5, respectively. Pine Island and Thwaites transects marked as in Fig. 1a (bounded by cyan and orange markers, respectively).



315 Across all RCP scenarios, the rate of bedrock uplift at the Thwaites and Pine Island
316 grounding lines in the Maxwell model (proximate to the orange- and cyan-filled circles,
317 respectively in Fig. 5), are on the order of magnitude of observed bedrock uplift rates in the ASE
318 (Lucas et al., 2024; SM-4). When transient deformation is included, the modelled rates of
319 bedrock uplift exceed that of the Maxwell model by an additional 10 to 40 mm/yr (Fig. 5b,d,f).

320 **3.2 Deviation in global mean sea level contribution**

321 The spatial pattern of global sea-level change is largely unaffected by transient solid Earth
322 rheology outside of Antarctica. The total amount of GMSL rise from the Antarctic Ice Sheet (AIS)
323 as a whole is dominated by the contribution from the WAIS, since majority of the ice loss occurs
324 in marine-grounded areas. Fig. 6 shows the transient–Maxwell deviation in GMSL rise contributed
325 by the WAIS over the course of the simulation, for all emissions scenarios. Examining the
326 deviation in the total WAIS GMSL contribution throughout the simulation (Fig. 6, right vertical
327 axis), we see that transient deformation causes the cumulative GMSL rise from the WAIS to be
328 smaller than that of the Maxwell model by several centimetres (~2 cm in RCP 2.6, ~3 cm in RCP
329 4.5, and ~5 cm in RCP 8.5). This is despite that the incremental WAIS GMSL contribution over a
330 given model time step is sometimes larger in the transient model (red fill, Fig. 6). The WAIS
331 GMSL contribution is reduced on the order of centimetres in the transient model relative to the
332 Maxwell model, regardless of which steady state viscosity profile is used (compare solid vs.
333 dashed continuous lines in Fig. 6). Even so, the percent reduction in both WAIS and AIS GMSL



334 contribution with transient deformation is ~5% or less for all times in the simulation; see SM-5 for
 335 absolute and percent deviations in WAIS GMSL contribution).

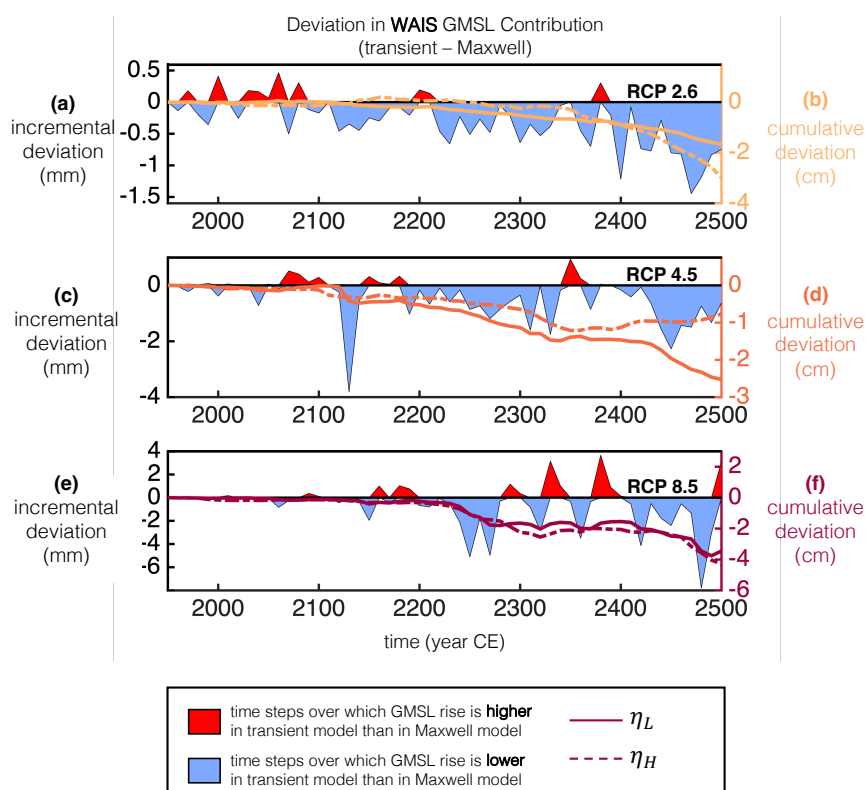


Figure 6. Deviation in WAIS GMSL Contribution (a),(c),(e) Blue and red filled lines indicate the associated Transient – Maxwell deviation in incremental GMSL contribution in millimetres from the WAIS over each time step in the simulations for RCP 2.6 (a), 4.5 (c) and 8.5 (e) forcings with steady state profile η_L . **(b),(d),(f)** Continuous lines indicate Transient – Maxwell deviation cumulative WAIS GMSL contribution in centimetres throughout the simulations using the η_L steady state profile (solid lines) and the η_H steady state viscosity (dashed lines) for RCP 2.6 (b), 4.5 (d) and 8.5 (f) forcings. For all RCP scenarios, the cumulative transient-Maxwell GMSL deviation is negative (reduction of total WAIS contribution to GMSL.)

336 4. Discussion and Conclusions

337 We simulate coupled Antarctic ice sheet–sea level dynamics with a 1D, radially varying
 338 GIA model (Gomez et al., 2010; Han et al., 2022; Kendall et al., 2005) and 3D ice sheet-shelf
 339 model (Pollard & Deconto, 2012; Pollard et al., 2015) subject to the RCP 2.6, 4.5, and 8.5
 340 emissions trajectories (IPCC, 2014). Our results show that transient rheology has a stabilizing
 341 effect on the WAIS by providing an additional (and earlier) strain contribution to solid Earth
 342 rebound in response to ice loss, thereby slowing and/or reducing the absolute extent of grounding
 343 line retreat. We observe differing sensitivities of grounding line retreat to transient deformation



344 between Pine Island Glacier and Thwaites Glaciers, likely because of the distinct roughness and
345 bathymetry profiles of the bedrock along the selected glacier transects. Overall, the local effects
346 of transient rheology are stabilizing to the WAIS via counteraction of the Marine Ice Sheet
347 Instability (MISI). We note that the stabilizing effects of transient deformation are only
348 temporary across WAIS grounding zones; over a timescale of centuries, both Maxwell and
349 transient simulations converge to similar magnitudes of grounding line retreat. That is, drastic ice
350 loss still occurs regardless of the assumed solid Earth rheology, but the pathway there varies.
351 This becomes the case for all RCP scenarios when rapid ice loss via the Marine Ice Cliff
352 Instability (MICI) is accounted for in the coupled ice sheet-sea level simulations (see Section
353 4.2). Although transient deformation cannot counteract the magnitude of projected global sea
354 level rise, the delayed trajectory of grounding line retreat with transient deformation on the
355 glacier-to-glacier scale aids in the interpretation of observations of change in the WAIS.
356 Moreover, predicted AIS discharge rates will play a role in understanding the global climate
357 feedbacks associated with the delivery of freshwater to the Southern Ocean (Gorte, 2023; Sadai
358 et al., 2025).

359 **4.1.1 Local feedback mechanisms and impact on global mean sea level**

360 As the WAIS shrinks throughout the simulation, water mass is added to the ocean and sea
361 level is lowered in the near field, due to both solid Earth uplift and reduced gravitational
362 attraction of the remaining ice load to the ocean. The counterpart of this local sea-level fall is
363 increased sea-level rise in the far field (Mitrovica et al., 2001). While ultimately, the contribution
364 of transient deformation to bedrock uplift prolongs the inevitable retreat and therefore integrated
365 GMSL rise (Gomez et al., 2015; Gomez et al., 2024), earlier in the simulations, the opposite is
366 true, i.e., our transient simulations show more incremental GMSL in the first few time steps. We
367 interpret this early opposing trend to be enhanced far field sea level rise due to increased water
368 expulsion in the transient simulations relative to the Maxwell (Fig 6; red fill). Despite this, there
369 is a net reduction in GMSL rise from Antarctica. The ability for solid Earth uplift to counteract
370 the MISI (or MICI) in West Antarctica builds with time as the simulation progresses, owing to
371 the time delay between the loading change and the associated strain contribution from non-
372 elastic deformation (see continuous lines, Fig. 6). We note that the magnitude of GMSL
373 reduction from transient deformation is small and likely within the uncertainty in dynamic ice
374 sheet model projections due to factors like basal conditions and implementation of ice sheet-shelf
375 physics (Bamber et al., 2022).

376 **4.1.2 Sensitivity to steady state viscosity**

377 As aforementioned, transient deformation affects the magnitude and timing of the solid
378 Earth response to loading changes, causing an apparent softening of Earth's mechanical
379 properties over relevant loading timescales and an effective reduction in time delay for viscous
380 deformation. In the Yamauchi and Takei (2016) rheological model, a given transient Earth model
381 is scaled to the assumed steady state viscosity profile and will therefore have a different
382 sensitivity to the timescale of the forcing than another transient Earth model scaled to a different
383 steady state viscosity profile. While we have chosen to focus our discussion on results based on
384 Earth structure characterized by the low (η_L) steady state viscosity profile, thought to be
385 representative of the hot structure beneath West Antarctica (Lloyd et al., 2020), there remains
386 substantial uncertainty in the absolute viscosity structure. Indeed, a lower Maxwell viscosity



387 mantle beneath West Antarctica is also consistent with GPS measurements of uplift rates. It is
388 unclear, however, whether these inferred low viscosities are representative of the long-term
389 viscosity as opposed to a transient deviation from a higher, steady state viscosity activated by
390 modern loading changes (Lau et al., 2021; Nield et al., 2025), or even some combination (see
391 SM-4, Fig. S5).

392 Given the uncertainty in steady state mantle viscosity, we also considered the coupled ice
393 sheet-sea level evolution of the WAIS with the high steady state viscosity profile for RCP 2.6,
394 RCP 4.5, and RCP 8.5 in West Antarctica. We find similar delayed trajectories of grounding line
395 retreat and magnitudes of the reduction in WAIS GMSL contribution with transient deformation
396 for both the low- and high steady state viscosity simulations (compare solid vs. dashed lines in
397 Fig. 6). For the low steady state viscosity profile, the WAIS GMSL contribution at 2500 is
398 reduced by 1.9% under RCP 8.5 (2.1% with high steady state viscosity profile), 4.1% under RCP
399 4.5 (1.7 % with high steady state viscosity profile), and 3.1% under RCP 2.6 (5% with high
400 steady state viscosity profile). These results suggest that the stabilizing effect of transient
401 deformation on grounding line retreat need not be unique to West Antarctica, given the
402 subglacial topography of some East Antarctic glaciers (Pritchard et al., 2025). There are several
403 marine-terminating outlet glaciers through which East Antarctica loses considerable ice mass,
404 and they have been suggested to exhibit considerable grounding line retreat (Favier et al., 2016;
405 Jones et al., 2015; Picton et al., 2023; Stokes, 2022).

406 **4.2 Impact of the Marine Ice Cliff Instability**

407 Though there is no consensus in physical treatment of calving, the Marine Ice Cliff Instability
408 (MICI) has been suggested to exacerbate both East and West Antarctic ice loss through rapid
409 cliff failure and the subsequent reduction in buttressing of upstream grounded ice (Bassis et al.,
410 2021; Bassis & Walker, 2012; Deconto et al., 2021; Golledge & Lowry, 2021; Pollard et al.,
411 2015). The transient Earth deformation response will be sensitive to such rapid loading changes,
412 and viscoelastic behaviour will occur on timescales that can better compete with that of ice loss,
413 thereby affecting the ice dynamics. We explore the potential effects of MICI on ice sheet-sea
414 level projections with transient Earth deformation (see SM-7; Supplementary Movies 5-6). We
415 find exacerbated deviations in grounding line position at a given time due to transient Earth
416 deformation in MICI simulations of RCP 2.6 and RCP 4.5. This reflects the expedited rate of ice
417 loss becoming sufficient to activate a larger transient deformation response. Under RCP 8.5,
418 however, when rapid ice loss via calving is invoked, there is minimal deviation in the grounding
419 line position between the transient and Maxwell models, precisely because the background
420 climate forcing is already sufficiently rapid to trigger the transient deformation response;



421 regardless of rheology, the solid earth uplift cannot keep pace with the ice sheet retreat, unlike in
 422 the more moderate climate scenarios.

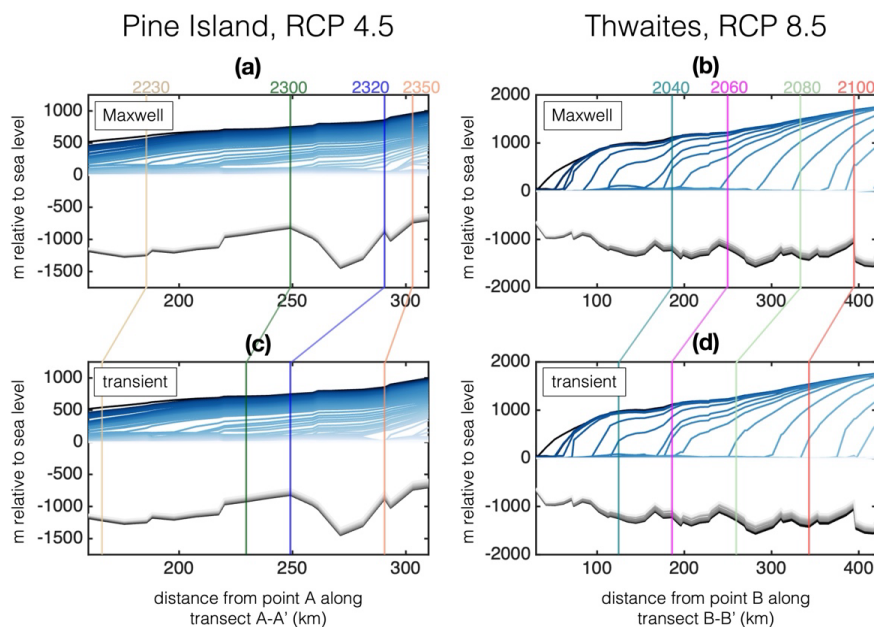


Figure 7. Deviation in Grounding line retreat with MICI Timeline of grounding line retreat across Pine Island and Thwaites Glaciers. Analogous to Fig. 2, instead using the coupled ice sheet-sea level simulations of RCP 4.5 with the inclusion of rapid ice calving via the MICI. Ice sheet (dark blue to light blue) and bedrock surface (dark grey to light grey) evolution at Pine Island Glacier (a,c) and Thwaites Glacier (b,d) for Maxwell and transient Earth models, respectively.

423 Fig. 7 is analogous to Fig. 2, illustrating grounding line retreat at Pine Island and
 424 Thwaites Glaciers for Maxwell versus transient Earth models, but with RCP 4.5 climate forcing
 425 and the additional consideration of MICI (implemented in the model via the algorithm described
 426 in DeConto & Pollard, et al. 2016 and DeConto et al., 2021). Fig. 7b,d demonstrates deviations
 427 in the Maxwell and transient model grounding line positions of between ~50-70 km at a given
 428 time in the simulation at Thwaites Glacier. While eventually the transient model catches up with
 429 the grounding line retreat in the Maxwell model by ~2130 CE, the trajectory is delayed. In the
 430 Maxwell model under RCP 4.5 with MICI included, Pine Island Glacier has nearly fully
 431 collapsed by 2380 CE (Fig. 7a). It takes another ~30 years for the glacier to fully retreat in the
 432 transient model. Given that understanding and modelling of calving processes is currently under
 433 active development in the literature, these results should be viewed as a preliminary sensitivity
 434 test of the role of transient deformation in modulating ice retreat through calving processes.
 435 Though we focus on West Antarctica, subglacial basins of East Antarctica are also prone to rapid
 436 retreat with MICI (Deconto et al., 2021). We see greater ice retention by upwards of 50 metres
 437 within the Wilkes, Aurora, and Recovery subglacial basins in the transient Earth rheology
 438 simulations as early as 2050 CE for all RCP simulations including MICI (see SM-6, Fig. S12).



439 Ultimately, the transient models with MICI catch up to the ice levels in the Maxwell simulations
440 with MICI after 2300 CE in East Antarctica (apart from a small region in the Wilkes Subglacial
441 Basin under RCP 8.5; Fig. S12). Given that Greenland, like East Antarctica, is predominantly
442 grounded above sea level and has cratonic mantle structure, we should also expect a delay in ice
443 retreat with transient Earth deformation.

444 **4.3 Moving to more realistic Earth rheology**

445 Although there is strong consensus in the rock physics community that transient viscous
446 deformation occurs over a range of timescales from the elastic end-member to the steady state
447 viscous regime, the exact nature of empirically-derived parametrizations of transient rheology
448 varies between laboratories (Faul & Jackson, 2015; Havlin et al., 2021; Lau & Holtzman, 2019;
449 Yamauchi & Takei, 2016). These transient models have differing sensitivities across the full
450 spectrum of loading timescales, and therefore predictions of sea level and ice sheet coevolution
451 with transient deformation will bear the uncertainty in the choice of transient model (as well as
452 the assumed trajectory of climate forcing).

453 Furthermore, Lau et al. (2025) model the GIA response to static ice loading changes
454 under future projections, accounting for lateral variations in both steady state mantle viscosity
455 and transient rheology (Yamauchi and Takei et al. 2016, as applied here though only to 1D Earth
456 models), but without consideration of dynamic ice sheet-sea level feedback. They find that
457 deviations in near field sea level from transient solid Earth deformation are on the order of or
458 larger than the effects of 3D Earth structure, suggesting that transient Earth rheology is an
459 important consideration in modelling modern and future marine grounding line dynamics.
460 Though the two distinct 1D steady state viscosity profiles used in this study are consistent in
461 terms of the magnitude of GMSL reduction in the transient Earth model relative to that of the
462 reference Maxwell model, future coupled ice sheet-sea level modelling studies should
463 incorporate laterally varying Earth structure (as in Gomez et al., 2024) in conjunction with
464 transient deformation behaviour, since East Antarctica and West Antarctica evolve
465 simultaneously and there is potential for covariance across the regions within the context of solid
466 Earth-ice sheet feedbacks (Gomez et al., 2018; Gomez et al., 2024; Lucas et al., 2024; van Calcar
467 et al., 2025). Moreover, this study considers the effects of complex time-dependent deformation
468 in the linear viscoelastic regime. There is also evidence for transient dislocation creep
469 mechanisms at these intermediate timescales (L. N. Hansen et al., 2021). Accordingly, stress-
470 dependence and transient deformation behaviour could also be considered together in regions of
471 high background stress (e.g., Lau et al. 2021).

472 Transient solid Earth deformation is unable to thwart the inevitable Antarctic ice loss and
473 sea level rise predicted in this coupled model of ice sheet-sea level-solid Earth interactions.
474 However, transient deformation has the potential to slow the pace of ice retreat and influence the
475 rate at which freshwater discharge from the Antarctic Ice Sheet is delivered to the ocean. All-the-
476 while, many studies from the atmospheric and oceanic modelling community (e.g. Sadai et al.
477 2020) have shown that freshwater outflux from the AIS can delay global temperature rise,
478 concurrently with increasing sea level rise, by driving the expansion of sea ice. Earth's albedo, or
479 reflectivity of the surface against solar radiation, is highly sensitive to sea ice extent and this
480 feedback has been shown to reduce predictions of global mean temperature between 0.3 and 1°C
481 by 2100 CE (Sadai et al., 2025). If we predict AIS evolution and contribution to sea-level rise
482 within the framework of transient solid Earth rheology, it remains unclear how the deviations
483 from Maxwell model predictions will impact ocean and atmospheric processes such as sea ice



484 growth and ocean circulation. Regardless, transient viscoelastic deformation is a more realistic
485 description of viscoelastic rock deformation behaviour. We demonstrate that transient earth
486 deformation delays AIS retreat, which controls the rate of freshwater discharge, thus it should be
487 a consideration in predicting and interpreting the response of the entire climate system.
488

489 **Code Availability**

490 All codes used in this study are publicly available from previously published studies. The sea
491 level model component of the coupled Ice Sheet-Sea Level model can be accessed at
492 https://github.com/hollyhan/1DSeaLevelModel_FWTW. The dynamic ice sheet model
493 component can be accessed at [https://www.frdr-dfdr.ca/repo/dataset/de1bb752-6778-4c5c-8293-
494 2abaddf93a89](https://www.frdr-dfdr.ca/repo/dataset/de1bb752-6778-4c5c-8293-2abaddf93a89)

495 **Data Availability**

496 The model outputs for ice sheet and sea level change, as well as the driver scripts for the
497 simulations will be made available in a repository prior to acceptance of the manuscript.
498
499

500 **Author Contribution**

501 A.N.C. developed the project. A.N.C. conducted the modelling with guidance from B.P. and
502 N.G. Results were analyzed by A.N.C. with guidance from B.P., N.G., H.C.P.L. The paper was
503 written by A.N.C. with feedback by B.P., H.C.P.L., N.G.
504

505 **Competing interests**

506 The authors declare they have no conflict of interest.
507

508 **Acknowledgements**

509 We thank N. Gomez for providing access and computation time on the Digital Resource Alliance
510 of Canada cluster and look forward to helpful feedback from the Editor and Reviewers.

511 **Financial Support**

512 This work was supported by the David and Lucile Packard Foundation and NSF grant EAR
513 2311897.
514

515 **References**

- 516 Abe-Ouchi, A., Saito, F., Kawamura, K., Raymo, M. E., Okuno, J. I., Takahashi, K., & Blatter, H.
517 (2013). Insolation-driven 100,000-year glacial cycles and hysteresis of ice-sheet volume.
518 *Nature*, 500(7461), 190-193. <https://doi.org/10.1038/nature12374>
519 Bamber, J. L., Oppenheimer, M., Kopp, R. E., Aspinall, W. P., & Cooke, R. M. (2022). Ice Sheet
520 and Climate Processes Driving the Uncertainty in Projections of Future Sea Level Rise:
521 Findings From a Structured Expert Judgement Approach. *Earth's Future*, 10(10).
522 <https://doi.org/10.1029/2022ef002772>
523 Barletta, V. R., Bevis, M., Smith, B. E., Wilson, T., Brown, A., Bordoni, A., Willis, M., Khan, S.
524 A., Rovira-Navarro, M., Dalziel, I., Smalley, R., Kendrick, E., Konfal, S., Caccamise, D.
525 J., Aster, R. C., Nyblade, A., & Wiens, D. A. (2018). Observed rapid bedrock uplift in



- 526 Amundsen Sea Embayment promotes ice-sheet stability. *Science*, 360(6395), 1335-1339.
527 <https://doi.org/10.1126/science.aao1447>
- 528 Bassis, J. N., Berg, B., Crawford, A. J., & Benn, D. I. (2021). Transition to marine ice cliff
529 instability controlled by ice thickness gradients and velocity. *Science*, 372(6548), 1342-
530 1344. <https://doi.org/10.1126/science.abf6271>
- 531 Bassis, J. N., & Walker, C. C. (2012). Upper and lower limits on the stability of calving glaciers
532 from the yield strength envelope of ice. *Proceedings of the Royal Society A: Mathematical,*
533 *Physical and Engineering Sciences*, 468(2140), 913-931.
534 <https://doi.org/10.1098/rspa.2011.0422>
- 535 Caron, L., Ivins, E., Larour, E., Adhikari, S., & Metivier, L. (2025). *Love number computation*
536 *within the Ice-sheet and Sea-level System Model (ISSM v4.24)*. Copernicus GmbH.
537 <https://dx.doi.org/10.5194/egusphere-2024-3414>
- 538 Coonin, A. N., Lau, H. C. P., & Coulson, S. (2025). Meltwater Pulse 1A sea-level-rise patterns
539 explained by global cascade of ice loss. *Nature Geoscience*, 18(3), 254-259.
540 <https://doi.org/10.1038/s41561-025-01648-w>
- 541 Deconto, R. M., & Pollard, D. (2016). Contribution of Antarctica to past and future sea-level rise.
542 *Nature*, 531(7596), 591-597. <https://doi.org/10.1038/nature17145>
- 543 Deconto, R. M., Pollard, D., Alley, R. B., Velicogna, I., Gasson, E., Gomez, N., Sadai, S., Condron,
544 A., Gilford, D. M., Ashe, E. L., Kopp, R. E., Li, D., & Dutton, A. (2021). The Paris Climate
545 Agreement and future sea-level rise from Antarctica. *Nature*, 593(7857), 83-89.
546 <https://doi.org/10.1038/s41586-021-03427-0>
- 547 Dziewonski, A. M., & Anderson, D. L. (1981). Preliminary reference Earth model. *Physics of the*
548 *Earth and Planetary Interiors*, 25(4), 297-356. [https://doi.org/10.1016/0031-](https://doi.org/10.1016/0031-9201(81)90046-7)
549 [9201\(81\)90046-7](https://doi.org/10.1016/0031-9201(81)90046-7)
- 550 Faul, U., & Jackson, I. (2015). Transient Creep and Strain Energy Dissipation: An Experimental
551 Perspective. *Annual Review of Earth and Planetary Sciences*, 43(1), 541-569.
552 <https://doi.org/10.1146/annurev-earth-060313-054732>
- 553 Faul, U. H., Fitz Gerald, J. D., Farla, R. J. M., Ahlefeldt, R., & Jackson, I. (2011). Dislocation
554 creep of fine-grained olivine. *Journal of Geophysical Research*, 116(B1).
555 <https://doi.org/10.1029/2009jb007174>
- 556 Favier, L., Pattyn, F., Berger, S., & Drews, R. (2016). Dynamic influence of pinning points on
557 marine ice-sheet stability: a numerical study in Dronning Maud Land, East Antarctica. *The*
558 *Cryosphere*, 10(6), 2623-2635. <https://doi.org/10.5194/tc-10-2623-2016>
- 559 Gолledge, N. R., & Lowry, D. P. (2021). Is the marine ice cliff hypothesis collapsing? *Science*,
560 372(6548), 1266-1267. <https://doi.org/10.1126/science.abj3266>
- 561 Gomez, N., Latychev, K., & Pollard, D. (2018). A Coupled Ice Sheet–Sea Level Model
562 Incorporating 3D Earth Structure: Variations in Antarctica during the Last Deglacial
563 Retreat. *Journal of Climate*, 31(10), 4041-4054. <https://doi.org/10.1175/jcli-d-17-0352.1>
- 564 Gomez, N., Pollard, D., & Holland, D. (2015). Sea-level feedback lowers projections of future
565 Antarctic Ice-Sheet mass loss. *Nature Communications*, 6(1), 8798.
566 <https://doi.org/10.1038/ncomms9798>
- 567 Gomez, N., Pollard, D., & Mitrovica, J. X. (2013). A 3-D coupled ice sheet – sea level model
568 applied to Antarctica through the last 40 ky. *Earth and Planetary Science Letters*, 384, 88-
569 99. <https://doi.org/10.1016/j.epsl.2013.09.042>
- 570 Gomez, N., Yousefi, M., Pollard, D., Deconto, R. M., Sadai, S., Lloyd, A., Nyblade, A., Wiens,
571 D. A., Aster, R. C., & Wilson, T. (2024). The influence of realistic 3D mantle viscosity on



- 572 Antarctica's contribution to future global sea levels. *Science Advances*, 10(31).
573 <https://doi.org/10.1126/sciadv.adn1470>
- 574 Gorte, T., Lovenduski, N. S., Nissen, C., & Lenaerts, J. T. M. (2023). Antarctic Ice Sheet
575 freshwater discharge drives substantial Southern Ocean changes over the 21st century.
576 *Geophysical Research Letters*, 50. <https://doi.org/10.1029/2023GL104949>
- 577 Gudmundsson, G. H. (2013). Ice-shelf buttressing and the stability of marine ice sheets. *The*
578 *Cryosphere*, 7(2), 647-655. <https://doi.org/10.5194/tc-7-647-2013>
- 579 Han, H. K., Gomez, N., Pollard, D., & Deconto, R. (2021). Modeling Northern Hemispheric Ice
580 Sheet Dynamics, Sea Level Change, and Solid Earth Deformation Through the Last Glacial
581 Cycle. *Journal of Geophysical Research: Earth Surface*, 126(4).
582 <https://doi.org/10.1029/2020jf006040>
- 583 Han, H. K., Gomez, N., & Wan, J. X. W. (2022). Capturing the interactions between ice sheets,
584 sea level and the solid Earth on a range of timescales: a new “time window” algorithm.
585 *Geoscientific Model Development*, 15(3), 1355-1373. [https://doi.org/10.5194/gmd-15-](https://doi.org/10.5194/gmd-15-1355-2022)
586 [1355-2022](https://doi.org/10.5194/gmd-15-1355-2022)
- 587 Hansen, K., Truffer, M., Aschwanden, A., Mankoff, K., Bevis, M., Humbert, A., Van Den Broeke,
588 M. R., Noël, B., Bjørk, A., Colgan, W., Kjær, K. H., Adhikari, S., Barletta, V., & Khan, S.
589 A. (2021). Estimating Ice Discharge at Greenland's Three Largest Outlet Glaciers Using
590 Local Bedrock Uplift. *Geophysical Research Letters*, 48(14).
591 <https://doi.org/10.1029/2021gl094252>
- 592 Hansen, L. N., Wallis, D., Breithaupt, T., Thom, C. A., & Kempton, I. (2021). Dislocation Creep
593 of Olivine: Backstress Evolution Controls Transient Creep at High Temperatures. *Journal*
594 *of Geophysical Research: Solid Earth*, 126(5). <https://doi.org/10.1029/2020jb021325>
- 595 Havlin, C., Holtzman, B. K., & Hopper, E. (2021). Inference of thermodynamic state in the
596 asthenosphere from anelastic properties, with applications to North American upper
597 mantle. *Physics of the Earth and Planetary Interiors*, 314, 106639.
598 <https://doi.org/10.1016/j.pepi.2020.106639>
- 599 IPCC. (2014). *Climate Change 2014: Synthesis Report. Contribution of Working Groups I, II and*
600 *III to the Fifth Assessment Report of the Intergovernmental Panel on Climate Change*
601 *[Core Writing Team, R.K. Pachauri and L.A. Meyer (eds.)]*.
- 602 Jones, R. S., Mackintosh, A. N., Norton, K. P., Golledge, N. R., Fogwill, C. J., Kubik, P. W.,
603 Christl, M., & Greenwood, S. L. (2015). Rapid Holocene thinning of an East Antarctic
604 outlet glacier driven by marine ice sheet instability. *Nature Communications*, 6(1), 8910.
605 <https://doi.org/10.1038/ncomms9910>
- 606 Kendall, R. A., Mitrovica, J. X., & Milne, G. A. (2005). On post-glacial sea level - II. Numerical
607 formulation and comparative results on spherically symmetric models. *Geophysical*
608 *Journal International*, 161(3), 679-706. <https://doi.org/10.1111/j.1365-246x.2005.02553.x>
- 609 Kopp, R. E., Deconto, R. M., Bader, D. A., Hay, C. C., Horton, R. M., Kulp, S., Oppenheimer, M.,
610 Pollard, D., & Strauss, B. H. (2017). Evolving Understanding of Antarctic Ice-Sheet
611 Physics and Ambiguity in Probabilistic Sea-Level Projections. *Earth's Future*, 5(12), 1217-
612 1233. <https://doi.org/10.1002/2017ef000663>
- 613 Larour, E., Seroussi, H., Adhikari, S., Ivins, E., Caron, L., Morlighem, M., & Schlegel, N. (2019).
614 Slowdown in Antarctic mass loss from solid Earth and sea-level feedbacks. *Science*,
615 364(6444), eaav7908. <https://doi.org/10.1126/science.aav7908>



- 616 Lau, H. C. P. (2023). Transient rheology in sea level change: Implications for Meltwater Pulse 1A.
617 *Earth and Planetary Science Letters*, 609, 118106.
618 <https://doi.org/10.1016/j.epsl.2023.118106>
- 619 Lau, H. C. P. (2024). Surface loading on a self-gravitating, linear viscoelastic Earth: moving
620 beyond Maxwell. *Geophysical Journal International*, 237(3), 1842-1857.
621 <https://doi.org/10.1093/gji/ggae149>
- 622 Lau, H. C. P., Austermann, J., Holtzman, B. K., Havlin, C., Lloyd, A. J., Book, C., & Hopper, E.
623 (2021). Frequency Dependent Mantle Viscoelasticity via the Complex Viscosity: Cases
624 From Antarctica. *Journal of Geophysical Research: Solid Earth*, 126(11).
625 <https://doi.org/10.1029/2021jb022622>
- 626 Lau, H. C. P., & Holtzman, B. K. (2019). “Measures of Dissipation in Viscoelastic Media”
627 Extended: Toward Continuous Characterization Across Very Broad Geophysical Time
628 Scales. *Geophysical Research Letters*, 46(16), 9544-9553.
629 <https://doi.org/10.1029/2019gl083529>
- 630 Lloyd, A. J., Wiens, D. A., Zhu, H., Tromp, J., Nyblade, A. A., Aster, R. C., Hansen, S. E., Dalziel,
631 I. W. D., Wilson, T. J., Ivins, E. R., & O’Donnell, J. P. (2020). Seismic Structure of the
632 Antarctic Upper Mantle Imaged with Adjoint Tomography. *Journal of Geophysical
633 Research: Solid Earth*, 125(3). <https://doi.org/10.1029/2019jb017823>
- 634 Lucas, E. M., Gomez, N., & Wilson, T. (2024). *The impact of regional-scale upper mantle
635 heterogeneity on glacial isostatic adjustment in West Antarctica*. Copernicus GmbH.
636 <https://dx.doi.org/10.5194/egusphere-2024-2957>
- 637 Mitrovica, J. X., Tamisiea, M. E., Davis, J. L., & Milne, G. A. (2001). Recent mass balance of
638 polar ice sheets inferred from patterns of global sea-level change. *Nature*, 409(6823), 1026-
639 1029. <https://doi.org/10.1038/35059054>
- 640 Nick, F. M., Van Der Veen, C. J., Vieli, A., & Benn, D. I. (2010). A physically based calving
641 model applied to marine outlet glaciers and implications for the glacier dynamics. *Journal
642 of Glaciology*, 56(199), 781-794. <https://doi.org/10.3189/002214310794457344>
- 643 Nield, G. A., Bentley, M. J., Koulali, A., Clarke, P. J., King, M. A., Wilson, T., & Whitehouse, P.
644 L. (2025). Surface Mass Balance Variability Causes Viscoelastic Solid Earth Deformation
645 in the Antarctic Peninsula. *Geophysical Research Letters*, 52(12).
646 <https://doi.org/10.1029/2025gl114595>
- 647 Picton, H. J., Stokes, C. R., Jamieson, S. S. R., Floricioiu, D., & Krieger, L. (2023). Extensive and
648 anomalous grounding line retreat at Vanderford Glacier, Vincennes Bay, Wilkes Land,
649 East Antarctica. *The Cryosphere*, 17(8), 3593-3616. [https://doi.org/10.5194/tc-17-3593-
650 2023](https://doi.org/10.5194/tc-17-3593-2023)
- 651 Pollard, D., & Deconto, R. M. (2012). Description of a hybrid ice sheet-shelf model, and
652 application to Antarctica. *Geoscientific Model Development*, 5(5), 1273-1295.
653 <https://doi.org/10.5194/gmd-5-1273-2012>
- 654 Pollard, D., Deconto, R. M., & Alley, R. B. (2015). Potential Antarctic Ice Sheet retreat driven by
655 hydrofracturing and ice cliff failure. *Earth and Planetary Science Letters*, 412, 112-121.
656 <https://doi.org/10.1016/j.epsl.2014.12.035>
- 657 Pollard, D., Gomez, N., & Deconto, R. M. (2017). Variations of the Antarctic Ice Sheet in a
658 Coupled Ice Sheet-Earth-Sea Level Model: Sensitivity to Viscoelastic Earth Properties.
659 *Journal of Geophysical Research: Earth Surface*, 122(11), 2124-2138.
660 <https://doi.org/10.1002/2017jf004371>



- 661 Pritchard, H. D., Fretwell, P. T., Fremand, A. C., Bodart, J. A., Kirkham, J. D., Aitken, A., Bamber,
662 J., Bell, R., Bianchi, C., Bingham, R. G., Blankenship, D. D., Casassa, G., Christianson,
663 K., Conway, H., Corr, H. F. J., Cui, X., Damaske, D., Damm, V., Dorschel, B.,...Zirizzotti,
664 A. (2025). Bedmap3 updated ice bed, surface and thickness gridded datasets for Antarctica.
665 *Scientific Data*, 12(1). <https://doi.org/10.1038/s41597-025-04672-y>
- 666 Sadai, S., Condron, A., Deconto, R., & Pollard, D. (2020). Future climate response to Antarctic
667 Ice Sheet melt caused by anthropogenic warming. *Science Advances*, 6(39), eaaz1169.
668 <https://doi.org/10.1126/sciadv.aaz1169>
- 669 Sadai, S., Karmalkar, A. V., Pollard, D., Dong, Y., Lucas, E., Gomez, N., Deconto, R., & Condron,
670 A. (2025). Antarctic meltwater alters future projections of climate and sea level. *Nature*
671 *Communications*, 16(1). <https://doi.org/10.1038/s41467-025-64438-3>
- 672 Schoof, C. (2007). Ice sheet grounding line dynamics: Steady states, stability, and hysteresis.
673 *Journal of Geophysical Research: Earth Surface*, 112(F3).
674 <https://doi.org/10.1029/2006jf000664>
- 675 Sergienko, O. (2025). Treatment of the ice-shelf backpressure and buttressing in two horizontal
676 dimensions. *Journal of Glaciology*, 71, 1-40. <https://doi.org/10.1017/jog.2024.83>
- 677 Sergienko, O., & Wingham, D. J. (2024). Diverse behaviors of marine ice sheets in response to
678 temporal variability of the atmospheric and basal conditions. *Journal of Glaciology*, 70, 1-
679 12. <https://doi.org/10.1017/jog.2024.43>
- 680 Spada, G., Ruggieri, G., Sørensen, L. S., Nielsen, K., Melini, D., & Colleoni, F. (2012). Greenland
681 uplift and regional sea level changes from ICESat observations and GIA modelling.
682 *Geophysical Journal International*, 189(3), 1457-1474. [https://doi.org/10.1111/j.1365-
683 246x.2012.05443.x](https://doi.org/10.1111/j.1365-246x.2012.05443.x)
- 684 Stokes, C. R., Abram, N.J., Bentley, M.J. et al. (2022). Response of the East Antarctic Ice Sheet
685 to past and future climate change. *Nature*(608), 275-286.
686 <https://doi.org/https://doi.org/10.1038/s41586-022-04946-0>
- 687 Thomas, R. H. (1979). The Dynamics of Marine Ice Sheets. *Journal of Glaciology*, 24(90), 167-
688 177. <https://doi.org/10.3189/s0022143000014726>
- 689 van Calcar, C. J., Bernales, J., Berends, C. J., van der Wal, W., & van de Wal, R. S. W. (2025).
690 Bedrock uplift reduces Antarctic sea-level contribution over next centuries. *Nature*
691 *Communications*, 16(1), 10512. <https://doi.org/10.1038/s41467-025-66435-y>
- 692 Weertman, J. (1974). Stability of the Junction of an Ice Sheet and an Ice Shelf. *Journal of*
693 *Glaciology*, 13(67), 3-11. <https://doi.org/10.3189/s0022143000023327>
- 694 Whitehouse, P. L., Bentley, M. J., Milne, G. A., King, M. A., & Thomas, I. D. (2012). A new
695 glacial isostatic adjustment model for Antarctica: calibrated and tested using observations
696 of relative sea-level change and present-day uplift rates. *Geophysical Journal*
697 *International*, 190(3), 1464-1482. <https://doi.org/10.1111/j.1365-246x.2012.05557.x>
- 698 Yamauchi, H., & Takei, Y. (2016). Polycrystal anelasticity at near-solidus temperatures. *Journal*
699 *of Geophysical Research: Solid Earth*, 121(11), 7790-7820.
700 <https://doi.org/10.1002/2016jb013316>
- 701 Zeitz, M., Haacker, J. M., Donges, J. F., Albrecht, T., & Winkelmann, R. (2022). Dynamic regimes
702 of the Greenland Ice Sheet emerging from interacting melt–elevation and glacial isostatic
703 adjustment feedbacks. *Earth System Dynamics*, 13(3), 1077-1096.
704 <https://doi.org/10.5194/esd-13-1077-2022>